Carpathian Journal of Earth and Environmental Sciences, February 2018, Vol. 13, No. 1, p. 161 – 174; DOI:10.26471/cjees/2018/013/015

TEXTURAL AND GEOCHEMICAL CHARACTERISTICS OF BEACH SANDS ALONG THE WESTERN GULF OF MEXICO, MEXICO

Violeta HERNÁNDEZ-HINOJOSA[1], Patricia C. MONTIEL-GARCÍA[2], John S. ARMSTRONG-ALTRIN[3*], Ramasamy NAGARAJAN[4] & Juan J. KASPER-ZUBILLAGA[3]

[1]Licenciatura en Ingeniería en Geología Ambiental, Área Académica de Ciencias de la Tierra y Materiales, Universidad Autónoma del Estado de Hidalgo, Mineral de la Reforma, Hidalgo; México; violeta.hhgeo@gmail.com
[2]Laboratorio de Geoquímica, Área Académica de Ciencias de la Tierra y Materiales, Universidad Autónoma del Estado de Hidalgo, Ciudad Universitaria, Carretera Pachuca-Tulancingo, Km 4.5, Col. Carboneras, C.P. 42184, Mineral de la Reforma, Hidalgo. México; patricia_montiel@hotmail.com
*[3]Universidad Nacional Autónoma de México, Unidad de Procesos Oceánicos y Costeros, Instituto de Ciencias del Mar y Limnología, Circuito Exterior s/n, 04510 México, CDMX, México; *armstrong@cmarl.unam.mx*
[4]Department of Applied Geology, Faculty of Engineering and Science, Curtin University, Malaysia, 98009, Miri, Sarawak, Malaysia; nagarajan@curtin.edu.my

Abstract: The beach areas Esmeralda (EM) and La Mancha (LM) are located in the western part of the Gulf of Mexico. Here we studied the textural, petrological, and geochemical variations between the EM and LM beach sands to infer their provenance. The texture and petrographic analyzes indicated that the EM sands are fine-grained in size and abundant in quartz content. The SEM-EDS data revealed that the EM sands are abundant in heavy minerals like ilmenite and LM sands are enriched in zircon. SiO_2 content is higher in EM sand than in LM sand. The chemical index of alteration (CIA) revealed that the intensity of weathering in the beach areas was similar, varying from low to moderate. The chondrite normalized rare earth element (REE) patterns with negative Eu anomaly of the EM sands indicated a felsic provenance, whereas the absence of negative europium anomaly in the LM sands indicated its derivation from intermediate source rocks like andesite. The major element based multidimensional tectonic discrimination diagrams suggested a passive margin setting for the sediments from both beach areas. The compositional differences identified between the EM and LM beach areas suggested that longshore currents in the mixing and homogenization of sands are not significant.

Keywords: sand, provenance, weathering, SEM-EDS, geochemistry.

1. INTRODUCTION

The geochemical composition of clastic sediments has been widely used to infer the provenance (Almasoud et al., 2015; Ding et al., 2015; Zaid, 2015a; Varga et al., 2017), to evaluate the weathering history of the source area (Kermani et al., 2016; Rashid & Ganai, 2015; Ma et al., 2017), and to infer the tectonic environment (Verma & Armstrong-Altrin, 2013, 2016; Khan & Khan, 2015; Etemad-Saeed et al., 2015). Numerous studies identified that trace elements such as rare earth elements (REE) and Y, Th, Zr, Hf, Nb, Sc, Co, and Cr are most suited for provenance discrimination, because of their short residence time in seawater and secondary processes like diagenesis do not affect them (Cullers, 1994; Garzanti et al., 2014; El Asmi et al., 2015). Previous studies focused on the geochemical composition to infer provenance of beach sands along the coastal regions from the western Gulf of Mexico are very few. For example, Kasper-Zubillaga et al., (2013) studied the geochemistry of beach sands from the northern Gulf of Mexico and suggested that the beach sands are highly useful to identify the tectonic environment of a sedimentary basin. The heavy metal concentrations of the estuary sediments from the Gulf of Mexico were documented by Botello et al., (2015). Recently, Armstrong-Altrin et al., (2015) and

Armstrong-Altrin & Machain-Castillo (2016) discussed the provenance of continental slope sediments from the northwestern part of the Gulf of Mexico. However, the REE characteristics of beach sands from the western part of the Gulf of Mexico have not been documented.

This article discusses the texture, petrography, and geochemistry of the sand samples collected from the Esmeralda (EM) and La Mancha (LM) beach areas of the southwestern Gulf of Mexico. The objective of this study is to evaluate the compositional differences between the two beach areas as well as to investigate the intensity of chemical weathering, provenance, and tectonic environment.

2. STUDY AREA

The beach areas EM and LM are located at the latitude 20°23'23.15" N, longitude 96°55'10.39" W and latitude 19°35'49.53" N, longitude 96° 22'39.96" W, respectively, in Veracruz State, western part of the Gulf of Mexico (Fig. 1). Lithology of the EM beach area, corresponds to two major geological provinces: 1) consists of sedimentary rocks of the Sierra Madre Oriental deposited in a marine environment, which were deformed due to the Laramide orogeny and 2) Pleistocene and Holocene poorly consolidated sandstones of eolian and shoreline deposits, with large tracts of alluvium and lacustrine sediments. The lithology of the LM corresponds to the Sierra Madre Oriental province and the Trans-Mexican Volcanic Belt, which consists of the late Cenozoic volcano sedimentary and continental sequences. The Pliocene-Quaternary was characterized by volcanic rocks, predominantly intermediate composition like andesite (Fig. 1).

3. METHODOLOGY

Thirty sand samples were collected, 15 from EM and 15 from LM beach areas along the western Gulf of Mexico. The samples were collected in the place where the waves end. A one cm thick top layer of the beach sand was removed before collecting the samples.

3.1 Grain size

Grain-size analysis was carried out using a Ro-Tap WS Tyler model RX-812 using ASTM sieves 12, 20, 35, 40, 70, 120, 140 and 230. 40 g of each sample was sieved for an interval of 20 minutes (Folk, 1960). Cumulative curves were constructed to calculate the statistical grain-size parameters (mean, median, kurtosis, and standard deviation) by applying the equations of Folk & Ward (1957).

3.2 Petrography

Thirty thin sections, 15 from EM and 15 from LM, were prepared for the petrography study. The analysis was conducted in two phases, 1) point-counting method and 2) petrographic description. The point counts were done using both Gazzi-Dickinson (Gazzi, 1966; Dickinson, 1970) and standard methods. In each thin section, we counted 300 framework grains for total quartz [Q = Quartz grains], total feldspar [F = potash feldspar (k) + plagioclase (P)], total lithics (L), volcanic (Lv), sedimentary (Ls), metamorphic (Lm), plutonic (Lp), heavy minerals (HM), and biogenic components (B). Petrographic descriptions were made based on the results obtained from the optical microscope model Olympus BX41TF.

3.3. Mineralogy

The chemical composition of selected sand grains was studied by the PHILLIPS XL-30 SEM equipped with EDAX spectrometer (EDS) system. The sand mineralogy was studied using the Siemens D5000 X-ray Diffractometer.

3.4. Geochemistry

All 30 sand samples were analyzed for major, trace, and REE geochemistry. Major element concentrations were analyzed using a conventional XRF procedure. Powdered samples were heated to 110°C for 6 hours followed by heating in a muffle furnace at 1000°C for two hours to determine LOI (loss on ignition). Lithium tetraborate was mixed with the samples and heated to 1000°C to form a fused sample for XRF analysis with a Rigaku RIX-3000 equipped with Rh tube. Calibration curves were prepared using International reference materials mentioned by Lozano & Bernal (2005). Chemical analysis for major elements has precisions better than 5%. Major-element concentrations were recalculated to an anhydrous (LOI-free) basis and adjusted to 100% before interpretation. The trace and REE were analyzed by an Inductively Coupled Plasma Mass Spectrometer (ICP-MS) using a method given by Balaram et al. (1995).

The United States Geological Survey Standard, BCR-2 (Basalt, Columbia River) was used for calibration. Three analyses were made for each sample and averaged. The analytical precision for trace elements is better than 5%.

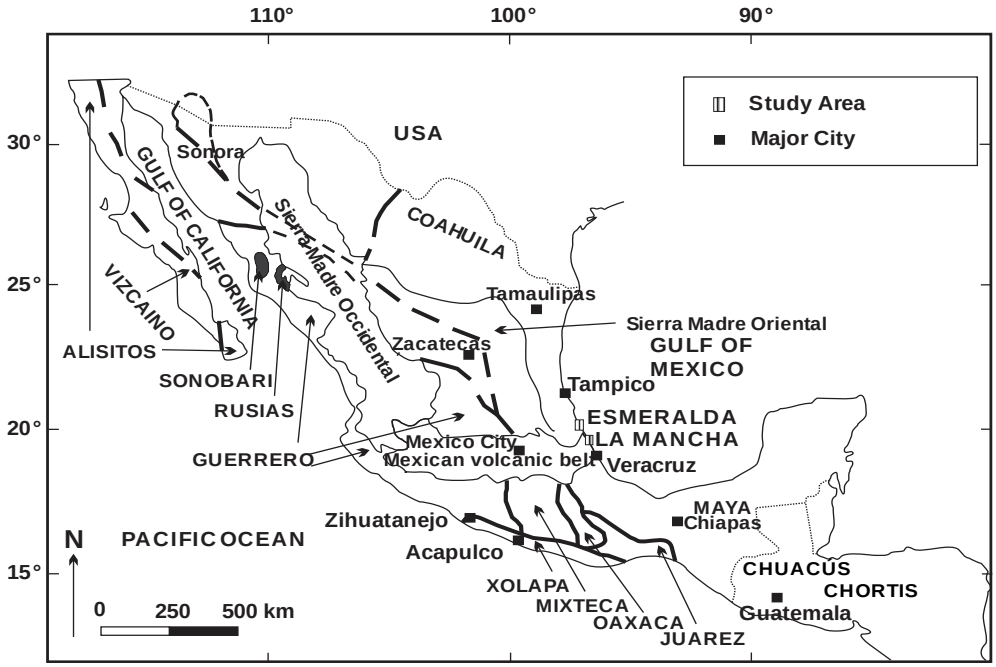

Figure 1. Map showing the location of the study area and terranes of Mexico (map modified after Armstrong-Altrin, 2009).

For the discussion of REE results, we used the upper continental crust (UCC) and chondrite normalization factors listed in Taylor & McLennan (1985). Eu anomaly (Eu/Eu^*) was calculated using the formula $Eu/Eu^* = Eu_N/[(Sm_N/Gd_N)]^{1/2}$; where $_N$ is the chondrite normalized value.

4. RESULTS

4.1 Grain size

The mean grain size ranges from ϕ 1.02 to ϕ 1.98 (0.5 mm to 0.24 mm) and ϕ 0.62 to ϕ 1.37 (0.65 mm to 0.39 mm) for the LM and EM sands, respectively, indicating that the sand grains are medium and coarse to medium-grained in size. The well sorted sands were probably formed when exposed to wave, which can reduce pore spaces among sand grains and improve their classification (Carranza-Edwards et al., 2009). Kasper-Zubillaga & Carranza-Edwards (2005) suggested that the fine-grained sands are well sorted due to the density selectivity of sand. Similarly, selectivity of wind produces well classified fine-grained sand, while mixing of eolian and marine processes generate variations in grain size (Kasper-Zubillaga, 2009). The EM sands are well sorted and indicating an eolian transport, while the LM sands are moderately sorted, indicating the combination of eolian, wave and abrasion processes that reduce the grain size and improve its classification (Madhavaraju et al., 2006; Armstrong-Altrin & Natalhy-Pineda, 2014). The medium-grained nature of the two beach sands reveals the passive margin tectonic environment of the study area.

The sands of the EM and LM are mostly well sorted. Their sorting homogeneity can be explained by the domination of laminar currents in the beach zone. The classification of sediments depends on their transport distance and depositional condition, which may cause well and/or poorly sorted classifications. Cordoba-Saldaña (2011) reported that exhaustion is dominant in wind processes, which could be responsible for the well sorted nature.

In EM sands, the range of asymmetry values is high, which indicates that the conditions of erosion, transport and sedimentation were not uniform during deposition. In contrast, LM sands show homogeneity in the asymmetry values. The negative asymmetry value obtained for the two beach sands indicates the domination of coarse-grained sand. However, combination of positive and negative values indicates a region with high energy condition.

The kurtosis values in the EM and LM sands vary from ϕ 1.20 to ϕ 1.64 (0.4 to 0.33 mm; leptokurtic to very leptokurtic) and ϕ 1.00 to ϕ 1.76 (0.5 to 0.31 mm; very leptokurtic to mesokurtic), respectively. Folk & Ward (1957) have deduced that the unimodal sediments show a mesokurtic shape and sediments derived from different environments may result platykurtic.

4.2 Petrography

The EM and LM sands are mostly sub-angular to sub-round in shapes and are texturally

moderately mature. Lithic fragments in LM sands are lithic volcanic (Lv) associated with few sedimentary rock fragments (Ls), EM sands are predominantly sedimentary rock fragments (Ls).

The LM sands have the highest modal proportion of plagioclase (P) and heavy mineral (HM) grains. In contrast, EM sands are rich in plagioclase (P), heavy mineral (HM), and biogenic (B) grains. The average Q-F-L ratios are Q_{68}-F_{11}-L_{21} and Q_{84}-F_5-L_{11} for the LM and EM sands, respectively (Fig. 2).

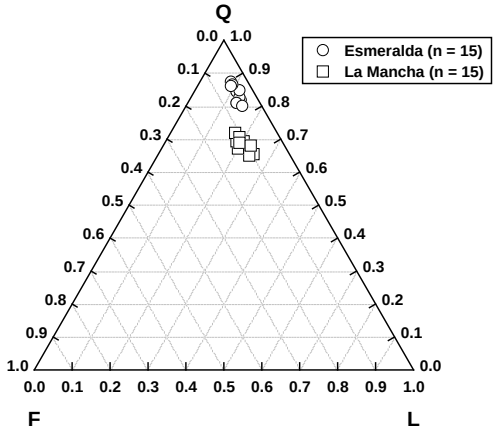

Figure 2. Q-F-L triangular diagram for the beach sands (Dickinson, 1985). Q = total quartz, F = total feldspar [K (potash feldspar) + P (plagioclase)], and L = total lithic fragments [volcanic (Lv) + sedimentary (Ls) + metamorphic (Lm) + plutonic (Lp)].

4.3 Mineralogy

The XRD study reveals that the LM sands are dominated by pyroxene, magnetite, and ilmenite grains. Similarly, using SEM-EDS method an ilmenite grain is identified in the EM sand (sample no. EM1), whereas in LM zircon grain is identified (Fig. 3).

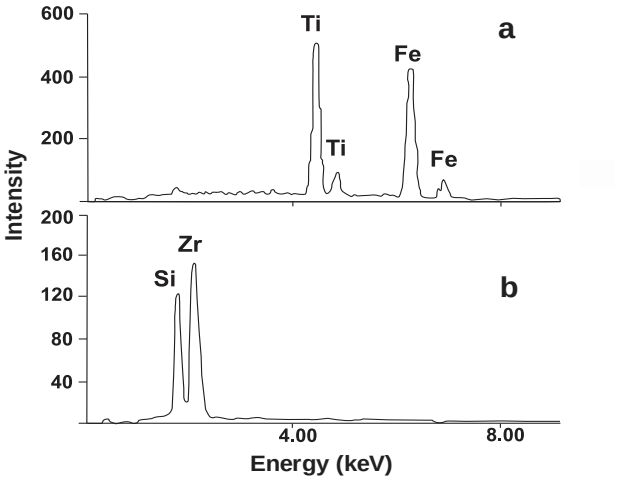

Figure 3. SEM - EDS spectrum for the beach sands. a) ilmenite (EM1); b) zircon (LM1).

4.4 Geochemistry

4.4.1 Major and trace element concentrations

The major and trace element concentrations for the EM and LM beach sands are listed in Tables 1 and 2, respectively. The EM sands have higher SiO_2 content (69-83 wt. %) than the LM sands (56-61 wt. %). Similarly, average Al_2O_3 content is slightly higher in LM sands (6.62-12.2 wt. %) than in EM sands (2.8-8.7 wt. %). In contrast, CaO and MgO contents are higher in LM than in EM sands. The variation in Na_2O (1.04-1.87 wt.%) and K_2O (1.21-2.45 wt.%) contents in EM sands is small, whereas it is large in the LM sands, ranging from 3.46 to 4.98 wt.% and 1.53 to 2.68 wt.%, respectively. The TiO_2, Fe_2O_3, MgO and CaO contents in LM sands are slightly elevated, which is probably due to the concentration of opaque minerals like magnetite and ilmenite (Tawfik et al., 2017).

On a log Fe_2O_3/K_2O vs log SiO_2/Al_2O_3 geochemical classification diagram (Herron, 1988) (Fig. 4), the EM sands are clustered in the litharenite field, whereas LM sands are plotted in the wake and Fe-sand fields, reflecting variations in the quartz and feldspar contents between the two beach areas.

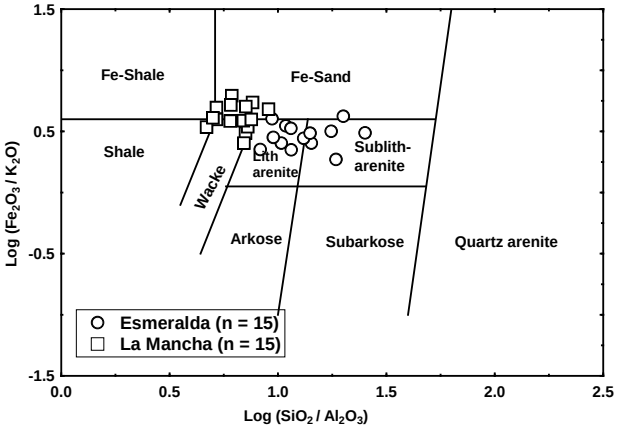

Figure 4. Geochemical classification diagram using log (SiO_2/Al_2O_3) – log (Fe_2O_3/K_2O) (Herron, 1972).

The UCC normalized trace element concentrations are showed in figure 5. In comparison with UCC, the Sc, Co, Cr, V, and Ni contents in EM are depleted, whereas Co, Cr, V, and Ni in LM sands are slightly elevated. The differences in trace element concentrations between the two beach areas are probably due to the variation in the type of source rocks.

4.4.2 Rare earth element concentrations

The REE content ranges from 36 to 78 ppm for the EM and 65-175 ppm for the LM sands, with

an average of 57 and 113 ppm, respectively (Table 3). The chondrite normalized REE patterns (Fig. 6) for the EM sands show LREE enriched and relatively flat HREE with a negative Eu anomaly ($Eu/Eu^* = 0.50$-0.77). However, the REE patterns for the LM sands are with slightly negative or without any Eu anomaly ($Eu/Eu^* = 0.71$-1.26).

This indicates a difference in the type of source rocks. Two samples from LM (LM6 and LM1) show highest REE content compared to other samples, which may be related to sorting of sediments during transportation or concentration of some minerals, probably zircon. The enrichment of heavy minerals in these samples is also identified by the SEM-EDS method (Fig. 3).

Similarly, ∑REE show a statistically significant correlation with Al_2O_3 for the LM sands ($r = 0.66$, $n = 15$), whereas this correlation is negative for the EM sands ($r = -0.17$, $n = 15$), which is due to the differences in the concentration of aluminosilicate minerals between the two beach areas (Li et al., 2016).

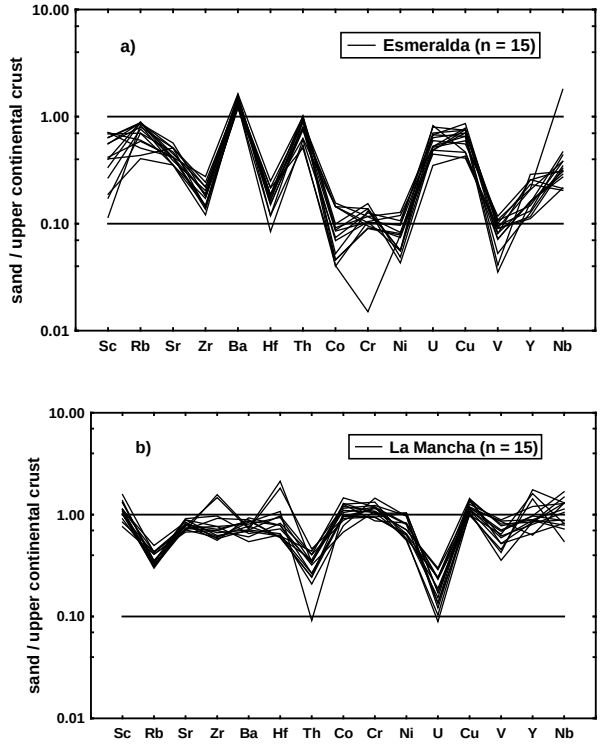

Figure 5. Multi-element diagram for trace element concentrations normalized against upper continental crust (Taylor & McLennan, 1985). a) Esmeralda (EM) sand; b) La Mancha (LM) sand.

5. DISCUSSION

5.1. Sediment maturity and recycling

The SiO_2/Al_2O_3 ratio is a widely-used to infer the textural maturity of sediments, where a high value represents compositionally matured sediments (Madhavaraju, 2015; Rashid et al., 2015). The average SiO_2/Al_2O_3 ratio in basic igneous rocks is 3, whereas it is about 5 in the acid igneous rocks, hence the values >5 in clastic sediments indicate sediment maturity (Armstrong-Altrin et al., 2012, 2013). The SiO_2/Al_2O_3 ratios vary from 8 to 25 and 5 to 9 in the EM and LM sands, respectively, indicating a moderate textural maturity. However, the textural maturity is higher for the EM sands compared to the LM ones.

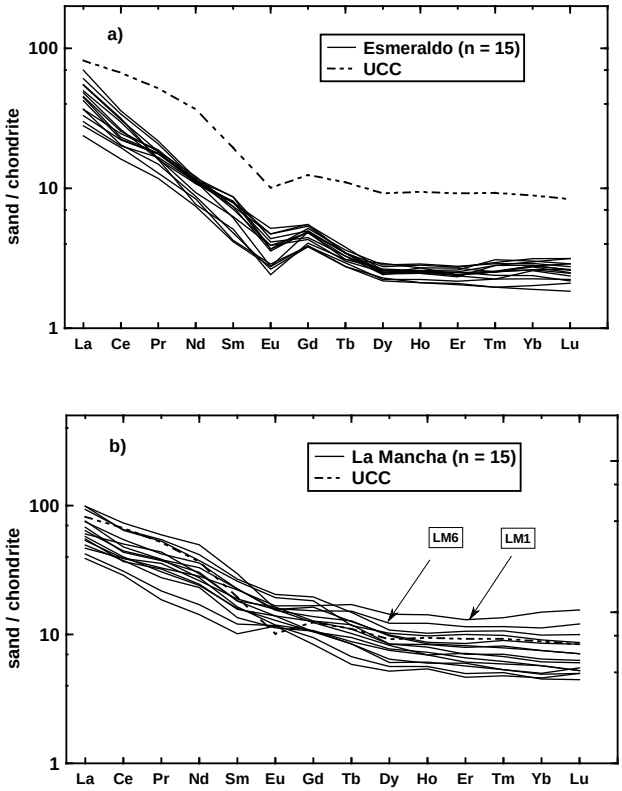

Figure 6. Chondrite-normalized rare earth element (REE) patterns. Chondrite normalization values are from Taylor & McLennan (1985). REE pattern of upper continental crust is also included for comparison. a) Esmeralda (EM) sand; b) La Mancha (LM) sand.

The Index of Chemical Variability ($ICV = Fe_2O_3 + K_2O + Na_2O + CaO + MgO + MnO + TiO_2) / Al_2O_3$ is also a measure to identify the compositional maturity of sediments, which was successfully applied in many studies (Cox et al., 1995; Armstrong-Altrin et al., 2014). Typical rock forming minerals like feldspars, amphiboles, and pyroxenes have ICV values of >1, whereas alteration products such as kaolinite, illite, and muscovite have ICV values <1 (Cox et al., 1995; Cullers, 2000). The average ICV values of EM (1.97 ± 0.76) and LM sands (2.70 ± 0.65) are >1 (Table 1). Compositionally immature sediments with high ICV values are first-cycle deposits, whereas

compositionally mature sediments consisting of low ICV values indicate high recycling and intensity of weathering (Van de Kamp & Leake, 1985). The difference in ICV values between the two beach areas indicates the compositional maturity is higher for the EM sands. The enrichment of Zr/Sc ratio in LM sands indicates that they are concentrated with zircon mineral.

5.2. Paleoweathering

Paleoweathering in the source region can be estimated through chemical index of alteration (CIA) (Nesbitt & Young, 1982). This weathering index has been extensively used in various studies (Armstrong-Altrin, 2009; Nagarajan et al., 2007a, 2007b; Bandopadhyay & Ghosh, 2015; Ramos-Vázquez et al., 2017). Chemical weathering strongly influences the mineralogy and major element composition of the sediments by removing labile cations such as $Ca^{2+,}$ Na^{+} and K^{+} relative to residual constituents (Al^{3+} and Ti^{4+}) through the conversion of feldspar to clay minerals (Nesbitt & Young, 1982; Selvaraj et al., 2016). Un-weathered igneous rocks have CIA values near to 50, whereas intensively weathered clay materials like kaolinite, gibbsite, and chlorite have values up to 100. In general, the CIA values are < 60, in the LM sands, which vary from 34 to 55, indicating low weathering. However, for the EM sands the CIA values vary from 40 to 72 (Table 1), indicate moderate weathering in the source area. Texturally, a significant enrichment in quartz (Q) and depletion in plagioclase (P) grains in EM sands supports this observation.

The CIA values for the EM and LM sands are plotted in the Al_2O_3-($CaO+Na_2O$)-K_2O(A-CN-K) ternary diagram, which permits to understand the variation in compositional changes due to chemical weathering and/or source rock composition (Fedo et al., 1995). On an A-CN-K ternary diagram (Fig. 7), the beach sands are plotted as two different groups, indicating the intensity of weathering is quite variable between the EM and LM sands.

The LM sands are clustered near the plagioclase-K-feldspar join line and to the average composition of andesite, whereas EM sands are closer to the average granodiorite source. This discrimination between the two beach areas reveals a weak to moderate weathering intensity in the source areas. The Th/U ratio is also used to measure the intensity of weathering for the beach sands, because weathering and recycling are expected to result in the oxidation of U^{4+} to the soluble U^{6+} state and its removal will increase the Th/U ratio above the average UCC value (Th/U = 3.8) (McLennan et al., 1993). The Th/U ratio values (> 3.8) for the EM and LM sands are indicating low to moderate weathering in the source area.

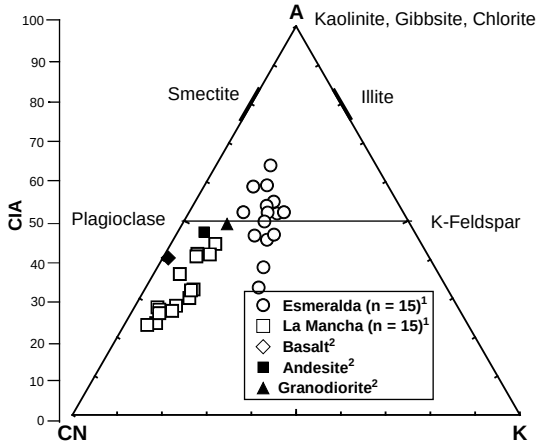

Figure 7. Ternary diagram to infer the intensity of weathering for EM and LM sands a) Al_2O_3 - (CaO^{*} + Na_2O) - K_2O (A-CN-K, in molecular proportion; Nesbitt & Young, 1982). Average rock composition of andesite, basalt, and granodiorite are from Condie (1993).

5.3. Provenance

Major and trace element concentrations of sediments can provide information about the provenance (Tetiker et al., 2015; Wen et al., 2016; Nagarajan et al., 2015). It is due to the reason that the chemical composition varies widely among sediments derived from felsic (dacite and granite), intermediate (andesite) and mafic (basalt) rocks (Verma et al., 2015, Verma, 2017). The REE and high field strength elements (HFSE) like Zr, Hf, Y, and Nb are particularly useful to discriminate the composition of the source rocks, because of their low mobility during weathering and transportation (Cullers, 2000). Also, the relative pattern and the size of the Eu anomaly were used to infer the nature of source rocks (Cullers, 1994; Armstrong-Altrin et al., 2014, 2016; Zhang & Gao, 2015). The major element based provenance discrimination diagram of Roser & Korsch (1988), was widely used in recent studies to discriminate the provenance of clastic sediments (Zaid, 2016). On this discriminant function diagram (Fig. 8) the LM sands plot in the intermediate and EM sands in the felsic igneous provenance fields which reveals a provenance difference between the two beach areas.

The high Rb content (> 40 ppm) in sediments is related to the felsic-intermediate igneous sources, whereas low Rb content (< 40 ppm) is related to mafic-intermediate source rocks (Wronkiewicz & Condie, 1990). In this study, the differences in Rb content between the LM (41 ± 7 ppm) and EM (80 ± 19 ppm) sands indicate that they were derived probably from intermediate and felsic source rocks, respectively.

Table 1. Major element concentrations in weight % for the Esmeralda (EM) and La Mancha (LM) beach sands, western Gulf of Mexico.

Muestra	SiO_2	TiO_2	Al_2O_3	Fe_2O_3	MnO	MgO	CaO	Na_2O	K_2O	P_2O_5	Total	CIA	ICV
EM-1	81.1	1.31	4.59	6.25	0.04	0.42	0.59	1.45	1.97	0.02	99.8	53.4	2.61
EM-2	78.3	0.78	5.68	5.62	0.01	0.32	0.56	1.26	2.01	0.01	99.8	59.7	1.86
EM-3	76.4	0.45	6.98	4.25	0.03	0.56	0.54	1.58	1.21	0.03	99.5	67.7	1.23
EM-4	79.2	0.59	4.26	4.56	0.01	0.45	1.35	1.12	2.45	0.03	99.3	46.4	2.47
EM-5	81.1	0.89	5.68	4.25	0.02	0.46	0.63	1.04	1.68	0.03	99.5	62.9	1.58
EM-6	78.0	0.91	7.52	5.41	0.03	0.78	0.58	1.87	2.13	0.01	99.8	62.2	1.55
EM-7	73.3	0.45	6.34	5.32	0.01	0.59	0.64	1.26	2.38	0.01	99.9	59.7	1.68
EM-8	72.7	0.26	8.69	4.25	0.02	0.56	0.87	1.45	1.89	0.01	99.7	67.3	1.07
EM-9	83.2	1.45	4.14	6.12	0.01	0.45	0.59	1.32	1.46	0.02	99.9	55.1	2.75
EM-10	74.3	0.56	5.62	6.79	0.02	0.25	0.64	1.63	2.45	0.01	99.9	54.3	2.19
EM-11	69.0	0.47	7.23	6.34	0.01	0.89	0.64	1.85	2.25	0.02	99.7	60.4	1.72
EM-12	74.6	0.78	5.26	5.38	0.02	0.46	0.52	1.49	1.76	0.01	99.9	58.2	1.98
EM-13	73.1	0.69	2.89	6.32	0.03	0.47	0.45	1.75	2.05	0.01	99.2	40.4	4.06
EM-14	73.4	0.71	6.35	4.56	0.01	0.89	0.74	1.82	1.36	0.02	99.6	61.8	1.59
EM-15	70.3	0.96	7.45	5.23	0.03	0.56	0.55	1.06	1.30	0.04	99.5	71.9	1.30
LM-1	60.5	0.62	6.62	8.56	0.06	1.25	6.56	4.56	1.78	0.12	99.1	33.9	3.52
LM-2	56.0	0.72	10.7	7.98	0.07	2.56	6.18	3.58	1.61	0.25	99.6	48.5	2.11
LM-3	57.4	0.65	7.46	8.36	0.05	2.24	9.56	3.46	1.53	0.14	99.9	33.9	3.46
LM-4	55.7	0.89	8.99	9.56	0.06	2.45	8.56	3.78	1.55	0.11	99.8	39.2	2.98
LM-5	61.3	1.56	11.6	7.46	0.04	1.89	4.67	3.64	1.89	0.08	99.9	53.4	1.81
LM-6	57.5	0.35	12.1	6.89	0.08	3.25	4.56	4.36	2.01	0.34	99.9	52.6	1.76
LM-7	54.0	0.56	8.90	9.25	0.06	2.63	7.69	4.87	1.78	0.07	99.4	38.2	3.01
LM-8	57.8	0.48	11.3	9.63	0.04	2.36	2.96	3.96	2.36	0.06	99.9	55.0	1.91
LM-9	59.0	0.69	8.33	7.56	0.06	1.45	5.89	4.78	2.48	0.14	99.9	38.7	2.74
LM-10	58.0	0.23	9.60	8.26	0.03	1.24	2.79	3.78	2.15	0.16	99.9	52.4	1.92
LM-11	60.0	0.45	8.59	6.79	0.40	2.35	4.98	3.65	2.68	0.25	99.4	43.1	2.43
LM-12	58.0	0.45	7.99	8.45	0.06	1.99	6.21	4.78	2.45	0.15	100	37.2	3.05
LM-13	54.0	1.12	7.79	10.3	0.31	4.56	3.87	4.98	2.65	0.75	99.9	40.3	3.52
LM-14	59.0	0.56	7.82	9.32	0.06	2.69	4.36	3.68	2.36	0.24	99.8	42.9	2.94
LM-15	57.0	0.45	8.01	8.96	0.05	3.25	7.39	4.35	1.78	0.26	99.7	37.1	3.27

CIA (Chemical Index of Alteration) = $[Al_2O_3/ [(Al_2O_3+CaO^*+Na_2O+K_2O)] \times 100$ (Nesbitt & Young, 1982);
ICV (Index of Chemical Variability)= $(Fe_2O+K_2O+Na_2O+CaO+MgO+MnO+TiO_2)/Al_2O_3$ (Cox et al., 1995).

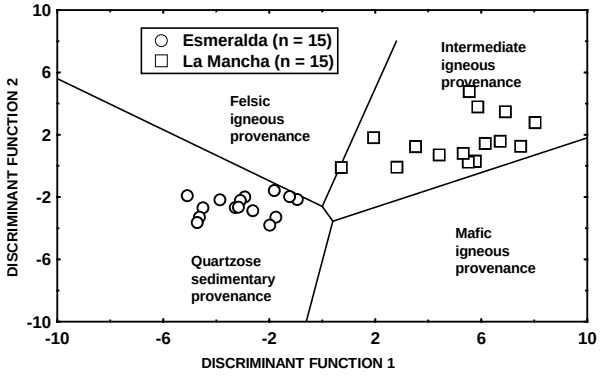

Figure 8. Major element based provenance discriminant function plot for the beach sands (Roser & Korsch, 1988). The discriminant functions are: Discriminant Function 1 = $(-1.773 \cdot TiO_2) + (0.607 \cdot Al_2O_3) + (0.760 \cdot Fe_2O_3) + (-1.500 \cdot MgO) + (0.616 \cdot CaO) + (0.509 \cdot Na_2O) + (-1.224 \cdot K_2O) + (-9.090$; Discriminant Function 2 = $(0.445 \cdot TiO_2) + (0.070 \cdot Al_2O_3) + (-0.250 \cdot Fe_2O_3) + (-1.142 \cdot MgO) + (0.438 \cdot CaO) + (1.475 \cdot Na_2O) + (1.426 \cdot K_2O) + (-6.861)$.

Similarly, trace elements like Sc, Th, Co, and La are highly useful to identify the provenance differences. The bivariate plot of Sc versus Th/Sc (Fig. 9) clearly reveals a provenance difference between the two beach areas. On this diagram EM sands plot near to the felsic and LM sands plot near to the intermediate rocks. This indicates that the EM sands were derived possibly by the felsic source rocks and LM sands from the intermediate source rocks.

The high contents of ferromagnesian trace elements like Cr, Ni, and V in sediments are indicative of a mafic provenance (Armstrong-Altrin et al., 2016). Garver et al. (1996) suggested that high Cr and Ni abundance (Cr > 150 ppm and Ni > 100 ppm) are indicative of ultramafic rocks in the source area.

Table 2. Trace element concentrations in ppm for the Esmeralda (EM) and La Mancha (LM) beach sands, western Gulf of Mexico

Sample	Ba	Cd	Co	Cr	Cu	Hf	Nb	Ni	Pb	Rb	Sc	Sr	Th	U	V	Y	Zn	Zr
EM-1	702	0.05	0.78	7.56	10.3	1.25	3.96	3.56	9.65	78.6	9.36	124	5.36	1.25	9.65	2.56	9.65	32.6
EM-2	685	0.04	0.69	1.25	11.6	0.69	3.48	3.45	2.45	65.9	5.69	146	5.69	1.36	7.68	3.56	11.5	25.8
EM-3	697	0.03	1.26	10.4	21.6	0.49	2.59	4.69	15.2	89.5	7.65	178	6.38	1.89	9.68	2.45	14.5	26.5
EM-4	789	0.02	2.45	11.4	14.9	0.89	4.56	2.46	9.56	96.4	8.65	198	7.89	1.45	11.5	3.24	10.2	34.2
EM-5	848	0.04	1.56	9.68	17.6	0.96	5.25	5.62	8.45	100	5.45	145	9.56	1.78	10.7	2.89	13.6	27.3
EM-6	770	0.12	2.45	8.4	18.7	0.87	3.69	4.36	6.56	98.6	8.69	135	8.36	2.24	8.69	3.46	16.3	38.4
EM-7	826	0.05	1.18	8.6	16.4	1.06	4.15	2.45	10.6	48.7	5.48	179	7.96	1.89	5.64	2.78	9.6	41.6
EM-8	679	0.04	2.45	7.89	19.0	1.08	3.26	3.26	3.56	57.0	9.68	147	6.59	1.35	7.65	3.56	8.5	27.9
EM-9	879	0.23	0.89	10.8	11.7	0.69	2.56	2.48	4.26	78.6	2.36	164	9.38	2.31	8.65	5.68	10.6	34.6
EM-10	796	0.15	1.48	11.4	10.7	1.08	4.59	1.89	3.26	98.6	4.58	157	10.3	0.98	9.78	4.57	11.7	41.8
EM-11	898	0.12	1.69	12.7	17.6	1.45	3.69	2.14	4.62	67.5	9.63	146	10.6	1.37	4.38	6.35	12.6	52.3
EM-12	770	0.21	2.65	9.65	16.4	1.26	5.61	3.65	10.6	98.6	7.56	177	9.48	1.48	3.78	3.45	14.2	46.3
EM-13	658	0.15	1.45	8.56	13.9	1.06	3.78	4.25	9.65	45.4	2.56	124	8.36	1.67	12.5	5.63	7.98	27.8
EM-14	759	0.26	0.68	8.69	19.6	0.97	2.46	5.26	8.56	85.5	3.65	145	9.89	1.47	10.7	5.12	8.69	36.1
EM-15	764	0.14	0.78	7.48	18.7	1.08	21.5	3.45	7.45	93.7	1.56	123	10.5	1.97	11.3	4.65	10.3	22.9
LM-1	410	0.03	21.6	110	25.7	12.35	15.6	25.6	6.45	45.7	13.5	245	3.56	0.25	45.6	38.6	45.3	299
LM-2	390	0.04	24.9	98.6	24.7	5.64	6.56	35.8	3.26	55.9	15.3	296	4.26	0.65	48.6	31.5	24.5	110
LM-3	426	0.06	21.9	85.4	26.6	3.48	10.6	45.8	4.25	48.6	11.4	278	2.56	0.48	38.7	18.6	45.6	116
LM-4	360	0.04	18.7	87.6	28.5	4.21	8.69	25.6	9.65	38.6	12.3	320	3.56	0.68	63.6	19.6	54.6	185
LM-5	489	0.15	16.3	95.4	24.7	3.45	9.78	35.2	10.6	39.6	17.8	248	2.56	0.38	68.9	35.4	55.7	175
LM-6	399	0.05	15.6	78.6	31.7	10.57	15.6	45.6	11.5	47.6	21.4	269	4.85	0.49	95.3	26.5	65.8	279
LM-7	445	0.45	19.6	102	34.7	5.46	17.9	43.0	12.4	36.6	18.6	259	3.58	0.38	86.5	18.3	75.6	145
LM-8	464	0.13	17.8	98.6	29.5	6.25	20.5	24.5	9.56	48.6	15.3	249	0.96	0.29	75.4	21.4	64.3	113
LM-9	513	0.06	16.9	78.3	27.4	4.56	15.6	28.6	13.6	35.5	15.4	279	2.78	0.67	55.9	18.6	47.6	106
LM-10	379	0.15	20.5	89.6	35.9	3.58	13.5	31.2	9.56	37.5	13.8	312	4.59	0.84	83.1	19.4	65.4	93.8
LM-11	479	0.05	21.4	61.2	33.8	3.48	12.5	36.5	7.89	34.4	14.6	256	3.78	0.67	65.9	17.6	35.7	125
LM-12	334	0.04	15.0	98.3	35.9	4.78	9.89	28.4	10.5	45.7	10.6	236	4.25	0.43	55.7	14.6	42.6	132
LM-13	299	0.03	16.3	78.4	27.6	3.69	10.6	27.6	8.69	34.3	13.7	312	2.78	0.53	73.4	21.6	51.4	145
LM-14	476	0.06	11.4	89.5	28.7	4.56	9.48	31.2	10.2	33.5	14.5	279	3.37	0.81	92.3	19.5	52.3	137
LM-15	390	0.07	13.2	121	29.8	3.78	15.6	42.5	12.5	39.6	17.9	286	2.19	0.34	91.7	13.7	38.6	126

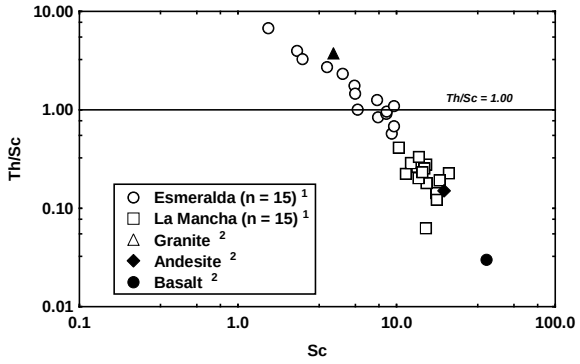

Figure 9. Bivariate plot of Sc-Th/Sc for the Esmeralda (EM) and La Mancha (LM) beach sands.

In this study, the slightly higher Cr, Ni, and V contents in the LM sands could be the result of contribution of sediments derived from intermediate source rocks. This observation is further supported by the Ni-Th*10-V ternary diagram (Fig. 10) (Bracciali et al., 2007), in which the LM sands revealed a contribution of sediments from intermediate source rocks. The average concentrations of dacite, andesite, and basalt rocks are from Condie (1993).

In addition, the REE pattern of the source rocks located nearer to the study areas were compared with the REE patterns of the EM and LM sands (Fig. 11). The compared rock types include basaltic-andesite, andesite and dacite. The EM sands are comparable with dacite composition (felsic), whereas the REE patterns of LM sands are comparable with basaltic andesite and andesite. Overall, the results and comparison of REE patterns reveal that the EM sands are dominated by sediments derived from the felsic igneous source rocks and LM sands from intermediate source rocks.

Table 3. Rare earth element concentrations in ppm for the Esmeralda (EM) and La Mancha (LM) beach sands, western Gulf of Mexico.

Muestra	La	Ce	Pr	Nd	Sm	Eu	Gd	Tb	Dy	Ho	Er	Tm	Yb	Lu	tREE
EM-1	25.6	34.2	2.98	8.42	2.00	0.32	1.58	0.21	1.08	0.25	0.69	0.10	0.72	0.11	78.3
EM-2	17.6	25.1	2.21	5.46	1.18	0.21	1.24	0.18	1.11	0.23	0.67	0.09	0.65	0.10	56.0
EM-3	8.69	15.4	1.61	5.28	0.96	0.24	1.19	0.16	0.83	0.18	0.51	0.07	0.50	0.08	35.7
EM-4	10.9	19.2	2.28	7.89	1.71	0.41	1.64	0.20	0.96	0.21	0.58	0.10	0.74	0.12	47.0
EM-5	15.4	21.4	2.42	8.25	1.64	0.34	1.47	0.19	0.92	0.22	0.59	0.08	0.64	0.09	53.7
EM-6	19.9	29.5	2.51	7.68	1.82	0.36	1.36	0.19	0.98	0.22	0.65	0.11	0.75	0.11	66.2
EM-7	10.2	18.6	1.76	5.98	0.98	0.25	1.18	0.17	0.85	0.19	0.54	0.08	0.56	0.09	41.5
EM-8	16.5	24.4	2.51	8.65	1.71	0.31	1.51	0.20	0.93	0.21	0.60	0.09	0.68	0.10	58.5
EM-9	22.2	32.4	2.84	8.12	2.01	0.38	1.52	0.20	1.05	0.24	0.68	0.11	0.78	0.12	72.8
EM-10	12.1	21.2	2.41	7.91	1.82	0.45	1.68	0.22	0.99	0.22	0.60	0.09	0.69	0.10	50.5
EM-11	13.4	19.5	2.04	6.23	1.11	0.23	1.17	0.16	0.87	0.18	0.52	0.07	0.47	0.07	46.1
EM-12	16.3	22.1	2.44	7.98	1.42	0.24	1.49	0.20	0.94	0.23	0.60	0.09	0.65	0.09	54.8
EM-13	13.4	23.5	2.58	8.09	1.84	0.41	1.69	0.20	0.99	0.21	0.63	0.10	0.70	0.10	54.5
EM-14	20.2	30.2	2.20	7.68	1.87	0.32	1.48	0.18	1.01	0.22	0.62	0.09	0.69	0.09	66.9
EM-15	18.2	28.4	2.24	6.62	1.45	0.34	1.32	0.18	0.96	0.22	0.63	0.09	0.59	0.08	61.4
LM-1	17.1	37.2	4.50	20.1	5.12	1.45	5.12	0.99	5.47	1.21	3.24	0.48	3.70	0.59	106
LM2	22.1	48.2	5.98	21.0	4.21	1.42	3.89	0.69	3.21	0.71	1.98	0.29	1.86	0.27	116
LM3	15.4	29.6	2.98	12.1	2.78	1.02	2.89	0.39	2.15	0.48	1.24	0.18	1.12	0.17	72.6
LM4	21.1	38.2	4.20	17.1	3.68	1.12	3.21	0.49	2.31	0.52	1.42	0.19	1.22	0.19	95.0
LM5	34.2	62.4	7.45	29.5	6.21	1.78	5.98	0.86	4.12	0.87	2.64	0.38	2.45	0.38	160
LM6	36.2	70.1	8.12	35.2	6.83	1.38	4.67	0.88	4.65	1.04	2.86	0.41	2.79	0.46	176
LM7	23.4	42.5	5.21	23.4	5.21	1.36	4.98	0.73	3.78	0.74	2.12	0.32	2.12	0.32	116
LM8	27.4	52.1	5.78	25.4	5.21	1.34	4.21	0.74	3.71	0.72	2.04	0.28	1.86	0.27	131
LM9	20.2	35.2	4.41	17.4	3.62	1.21	3.21	0.55	2.94	0.62	1.64	0.22	1.42	0.20	93.1
LM10	24.9	41.5	5.12	21.5	4.20	1.21	3.86	0.64	3.21	0.68	1.75	0.25	1.60	0.24	111
LM11	19.6	37.2	4.87	18.5	4.36	1.36	3.78	0.59	3.14	0.59	1.78	0.24	1.52	0.23	97.9
LM12	18.1	35.8	3.78	16.4	3.12	0.98	3.25	0.49	2.45	0.51	1.49	0.19	1.24	0.21	88.2
LM13	36.2	61.4	7.24	26.5	5.98	1.68	5.58	0.68	3.89	0.83	2.49	0.35	2.25	0.33	155
LM14	27.8	45.7	5.25	19.5	3.78	1.03	3.28	0.51	2.87	0.59	1.52	0.21	1.42	0.20	114
LM15	14.2	27.5	2.55	10.1	2.34	1.01	2.56	0.34	1.98	0.46	1.16	0.17	1.14	0.19	65.8

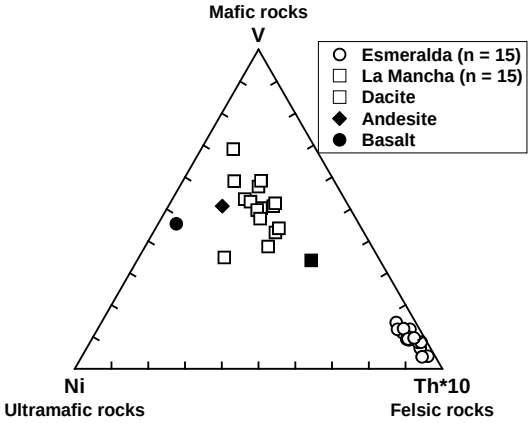

Figure 10. Ni-Th*10- V ternary diagram (Bracciali et al., 2007) for the Esmeralda (EM) and La Mancha (LM) beach sands. Average compositions of dacite, andesite, and basalt from the source area are also plotted for comparison; refer Figure 1 for source area and references.

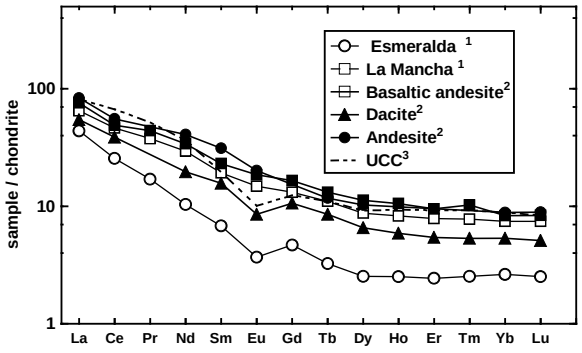

Figure 11. Average chondrite-normalized rare earth element (REE) patterns for the beach sands. n = number of samples; [1] Beach sands of this study; [2] REE patterns for average basaltic andesite, dacite, and andesite are from the source areas. [3] UCC = upper continental crust (Taylor & McLennan (1985);

5.4. Tectonic setting

The major-element based discrimination diagrams of Bhatia (1983) and Roser & Korsch (1986) for clastic sediments have been traditionally used in various studies to identify the tectonic setting of unknown basins (Zaid 2016; Periasamy & Venkateshwarlu, 2017). Although numerous studies identified the results inferred from these discrimination diagrams are inconsistent with the geology of the studied areas. Armstrong-Altrin and Verma (2005) evaluated these discrimination diagrams and showed a low percentage success rate (0%-23%) for the Bhatia (1983) diagram and 31.5%-52.3% for the Roser & Korsch (1986) diagram. Recently, based on the geochemical composition of Neogene-Quaternary sediments, Verma & Armstrong-Altrin (2013) proposed two discriminant function based major element diagrams for the tectonic discrimination of siliciclastic sediments for high-silica [$(SiO_2)_{adj}$ = 63%-95%] and low-silica [$(SiO_2)_{adj}$ = 35%-63%] types, from three main tectonic settings: island or continental arc, continental rift, and collision. In addition, Armstrong-Altrin (2015) evaluated these two tectonic discrimination diagrams and recommended that the two multidimensional diagrams can be considered as a tool for successfully discriminating the tectonic setting of older sedimentary basins. In fact, these discrimination diagrams were successfully used in recent studies to discriminate the tectonic setting of a source region based on clastic sediment geochemistry (Tobia & Aswad, 2015; Zaid, 2015b, c). On these high silica and low silica multidimensional diagrams (Fig. 12), the EM and LM sands are plotted in the rift field suggesting a passive margin, which is consistent with the geology of the Gulf of Mexico.

6. CONCLUSIONS

Textural and geochemical analyses of La Mancha (LM) and Esmeralda (EM) beach sands collected from the western Gulf of Mexico were studied to determine the provenance and tectonic setting of the source region. The LM sands were accompanied by different proportions of quartz (68%), feldspar (11%), and lithic fragments (21%), whereas EM sands were characterized by higher quartz with lower feldspar and lithic fragments (Q_{84}-F_5-L_{11}).

The XRD and SEM-EDS data revealed that the LM sands were abundant in heavy minerals like ilmenite and zircon. The REE concentration is higher in LM than EM sand, which is due to the concentration of heavy minerals in LM sands.

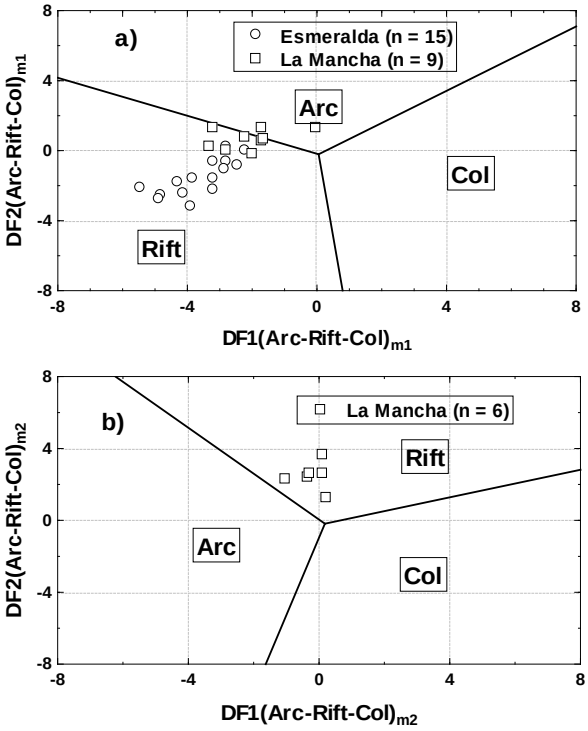

Figure 12. a) Discriminant-function multi-dimensional diagram for high-silica clastic sediments (Verma & Armstrong-Altrin, 2013). The subscript $_{m1}$ in DF1 and DF2 represents the high-silica diagram based on $\log_e$-ratios of major-elements. The discriminant function equations are: $DF1_{(Arc\text{-}Rift\text{-}Col)m1}$ = (– 0.263 × $In(TiO_2/SiO_2)_{adj}$) + (0.604 × In $(Al_2O_3/SiO_2)_{adj}$) + (– 1.725 × $In(Fe_2O_3t/SiO_2)_{adj}$) + (0.660 × $In(MnO/SiO_2)_{adj}$) + (2.191 × $In(MgO/SiO_2)_{adj}$) + (0.144 × $In(CaO/SiO_2)_{adj}$) + (– 1.304 × $In(Na_2O/SiO_2)_{adj}$) + (0.054 × $In(K_2O/SiO_2)_{adj}$) + (– 0.330 × $In(P_2O_5/SiO_2)_{adj}$) + 1.588; $DF2_{(Arc\text{-}Rift\text{-}Col)m1}$ = (– 1.196 × $In(TiO_2/SiO_2)_{adj}$) + (1.604 × $In(Al_2O_3/SiO_2)_{adj}$) + (0.303 × $In(Fe_2O_3^t/SiO_2)_{adj}$) + (0.436 × $In(MnO/SiO_2)_{adj}$) + (0.838 × $In(MgO/SiO_2)_{adj}$) + (– 0.407 × $In(CaO/SiO_2)_{adj}$) + (1.021 × $In(Na_2O/SiO_2)_{adj}$) + (– 1.706 × $In(K_2O/SiO_2)_{adj}$) + (– 0.126 × $In(P_2O_5/SiO_2)_{adj}$) – 1.068
b) Discriminant-function multi-dimensional diagram for low-silica clastic sediments (Verma & Armstrong-Altrin, 2013). The subscript $_{m2}$ in DF1 and DF2 represents the low-silica diagram based on $\log_e$-ratio of major elements. Discriminant function equations are: $DF1_{(Arc\text{-}Rift\text{-}Col)m2}$ = (0.608 × $In(TiO_2/SiO_2)_{adj}$) + (– 1.854 × $In(Al_2O_3/SiO_2)_{adj}$) + (0.299 × $In(Fe_2O_3^t/SiO_2)_{adj}$) + (– 0.550 × $In(MnO/SiO_2)_{adj}$) + (0.120 × $In(MgO/SiO_2)_{adj}$) + (0.194 × $In(CaO/SiO_2)_{adj}$) + (–1.510 × $In(Na_2O/SiO_2)_{adj}$) + (1.941 × $In(K_2O/SiO_2)_{adj}$) + (0.003 × $In(P_2O_5/SiO_2)_{adj}$) – 0.294; $DF2_{(Arc\text{-}Rift\text{-}Col)m2}$ = (– 0.554 × $In(TiO_2/SiO_2)adj$) + (– 0.995 × In $(Al_2O_3/SiO_2)_{adj}$) + (1.765 × $In(Fe_2O_3^t/SiO_2)_{adj}$) + (– 1.391 × $In(MnO/SiO_2)_{adj}$) + (– 1.034 × $In(MgO/SiO_2)_{adj}$) + (0.225 × $In(CaO/SiO_2)_{adj}$) + (0.713 × $In(Na_2O/SiO_2)_{adj}$) + (0.330 × $In(K_2O/SiO_2)_{adj}$) + (0.637 × $In(P_2O_5/SiO_2)^{adj}$) – 3.631

Major element concentrations suggested that the source rocks of the EM sands are more SiO_2 rich than those of the LM sands. The CIA values suggested that the weathering in the source area was low to moderate. Compared with LM sands the concentration of Co, Cr, Ni, and V are lower and La and Th are higher in the EM sands. This indicates that the LM and EM sands were derived from the intermediate and felsic source rocks, respectively.

The comparison of REE patterns to the source rocks also revealed the contribution of sediments from the intermediate and felsic rock types for the LM and EM sands, respectively. The major-element based discrimination diagrams showed a rift setting for the two beach areas. The compositional differences identified between the LM and EM beach areas suggested that longshore currents in the mixing and homogenization of sands are not significant.

Acknowledgments

JSA appreciate the financial assistance provided by the Programa de Apoyo a proyectos de Investigación e Innovación Tecnológica Project (no: IN106117). JSA is also grateful to the ICML, UNAM, Institutional project (no. 616) and "Cordinación de la Investigación Científica-UNAM" for the support for an academic stay at Annamalai University, India through an exchange program (COIC/STIA/8290/2017).

The authors are thankful to the laboratory technicians Susana Santiago-Perez, Eduardo Morales de la Garza, Ricardo Martinez, Arturo Ronquillo Arvizu, and Hector Mauricio Alexander Valdez for their help in the laboratory. We thank the staffs Patricia Girón García, Rufino SantaCruz, Carlos Linares-López, and Teodoro Hernández Treviño for XRD, XRF, SEM-EDS, and heavy mineral identification, respectively. Our special thanks to Lic. Arturo Ferrer Méndez Flores, librarian, UNAM for his consistent help to understand the geology of the Gulf of Mexico.

REFERENCES

Almasoud, F. I., Usman, A. R. & Al-Farraj, A. S., 2015. *Heavy metals in the soils of the Arabian Gulf coast affected by industrial activities: analysis and assessment using enrichment factor and multivariate analysis.* Arabian Journal of Geosciences, 8 (3), 1691-1703.

Armstrong-Altrin, J. S., 2009. *Provenance of sands from Cazones, Acapulco, and Bahía Kino beaches, Mexico*. Revista Mexicana de Ciencias Geologicas, *26*, 764-782.

Armstrong-Altrin, J. S., 2015. *Evaluation of two multi-dimensional discrimination diagrams from beach and deep-sea sediments from the Gulf of Mexico and their application to Precambrian clastic sedimentary rocks*. International Geology Review, 57, 1446-1461.

Armstrong-Altrin, J. S. & Verma, S. P., 2005. *Critical evaluation of six tectonic setting discrimination diagrams using geochemical data of Neogene sediment from known tectonic settings*. Sedimentary Geology, 177, 115-129.

Armstrong-Altrin, J.S. & Natalhy-Pineda, O. (2014). *Microtextures of detrital sand grains from the Tecolutla, Nautla, and Veracruz beaches, western Gulf of Mexico, Mexico: implications for depositional environment and palaeoclimate*. Arabian Journal of Geosciences, 7(10), 4321-4333.

Armstrong-Altrin, J. S. & Machain-Castillo, M. L., 2016. *Mineralogy, geochemistry, and radiocarbon ages of deep sea sediments from the Gulf of Mexico, Mexico*. Journal of South American Earth Sciences, vol. 71, pp. 182-200.

Armstrong-Altrin, J. S., Lee, Y. I., Kasper-Zubillaga, J. J., Carranza-Edwards, A., Garcia, D., Eby, N., Balaram, V. & Cruz-Ortiz, N. L., 2012. *Geochemistry of beach sands along the Western Gulf of Mexico: Implication for provenance*. Chemie der Erde - Geochemistry, 72, 345-362.

Armstrong-Altrin, J. S., Nagarajan, R., Madhavaraju, J., Rosales-Hoz, L., Lee, Y. I., Balaram, V., Cruz-Martinez, A. & Avila-Ramirez, G., 2013. *Geochemistry of the Jurassic and upper Cretaceous shales from the Molango Region, Hidalgo, Eastern Mexico; implications of source-area weathering, provenance, and tectonic setting.* Comptes Rendus Geosciences, 345, 185-202.

Armstrong-Altrin, J. S., Nagarajan, R., Lee, Y. I., Kasper-Zubillaga, J. J. & Córdoba-Saldaña, L. P., 2014. *Geochemistry of sands along the San Nicolás and San Carlos beaches, Gulf of California, Mexico: Implications for provenance and tectonic setting*. Turkish Journal of Earth Sciences, 23, 533-558.

Armstrong-Altrin, J. S., Nagarajan, R., Balaram, V. & Natalhy-Pineda O., 2015. *Petrography and geochemistry of sands from the Chachalacas and Veracruz beach areas, western Gulf of Mexico, Mexico: constraints on provenance and tectonic setting*. Journal of South American Earth Sciences, 64, 199-216.

Armstrong-Altrin, J. S., Lee, Y. I., Kasper-Zubillaga, J. J. & Trejo-Ramírez, E., 2016. *Mineralogy and geochemistry of sands along the Manzanillo and El Carrizal beach areas, southern Mexico: implications for palaeoweathering, provenance, and tectonic setting*. Geological Journal, DOI: 10.1002/gj2792.

Balaram, V., Anjaiah, K. V. & Reddy, M. R. P., 1995. *Comparative study on the trace and rare earth element analysis of an Indian polymetallic nodule reference sample by inductively coupled plasma atomic emission spectrometry and inductively coupled plasma mass spectrometry.* Analyst, 120, 1401-1406.

Bandopadhyay, P.C. & Ghosh, B., 2015. *Provenance*

analysis of the Oligocene turbidites (Andaman Flysch), South Andaman Island: a geochemical approach. Journal of Earth System Science, 124, 1019-1037.

Bhatia, M. R., 1983. *Plate tectonics and geochemical composition of sandstones*. Journal of Geology, *91*, 611-627.

Botello, A. V., Soto, L. A., Ponce-Vélez, G. & Villanueva, S.F., 2015. *Baseline for PAHs and metals in NW Gulf of Mexico related to the deep water horizon oil spill*. Estuarine Coastal Shelf Science, 156, 124-133.

Bracciali, L., Marroni, M., Pandolfi, L. & Rocchi, S., 2007. *Geochemistry and petrography of Western Tethys Cretaceous sedimentary covers (Corsica and Northern Apennines): from source area to configuration of margins*. Geological Society of America Special Paper, 420, 73-93.

Carranza-Edwards, A., Kasper-Zubillaga, J. J., Rosales-Hoz, L., Morales-De la Garza, E. & Santa Cruz, R. L., 2009. *Beach sand composition and provenance in a sector of the southwestern Mexican Pacific*. Revista Mexicana de Ciencias Geologicas, 26 (2), 433-447.

Condie, K.C., 1993. *Chemical composition and evolution of the upper continental crust: contrasting results from Surface samples and shales*. Chemical Geology, *104*, 1-37.

Cordoba-Saldaña, L. P., 2011. *Análisis granulométrico y geoquímico de arenas recientes en tres playas de México (Tecolutla, Bahia Kino y San Carlos): Implicación de procedencia*, MSc thesis, Posgrado en Ciencias del Mar y Limnología, UNAM, Mexico.

Cox, R., Lowe, D. R. & Cullers, R. L., 1995. *The influence of sediment recycling and basement composition on evolution of mudrock chemistry in the southwestern United States*. Geochimica et Cosmochimica Acta, 59, 2919-2940.

Cullers, R. L., 1994. *The controls on the major and trace element variation of shales, siltstones, and sandstones of Pennsylvanian-Permian age from uplifted continental blocks in Colorado to platform sediment in Kansas, USA*. Geochimica et Cosmochimica Acta, 58, 4955-4972.

Cullers, R. L., 2000. *The geochemistry of shales, siltstones, and sandstones of Pennsylvanian-Permian age, Colorado, USA: implications of provenance and metamorphic studies*. Lithos, 51, 181-203.

Dickinson, W. R., 1970. *Interpreting detrital modes of greywacke and arkose*. Journal of sedimentary petrology, 40, 695-707.

Dickinson, W. R., 1985. *Interpreting provenance relation from detrital modes of sandstones.* In: Zuffa G.G, editor. Provenance of Arenites: NATO ASI Series, C 148, D. Reidel Publishing Company, Dordrecht, pp. 333-363.

Ding, X., Tian, J., Chen, J., Yao, J., Deng, X. & Li, Y., 2015. *Paleogeographic framework and provenance features during Late Triassic Chang 9 time of the Yanchang Formation, Ordos Basin, China*. Arabian Journal of Geosciences, 8, 6731-6743.

El Asmi, A. M., Khaldi, H. & El Asmi, K., 2015. *Elemental geochemical compositions of shallow marine deposits: a proxy for correlation*. Arabian Journal of Geosciences, 8 (11), 10065-10092.

Etemad-Saeed, N., Hosseini-Barzi, M., Adabi, M.H., Hossein-Adabi, M., Sadeghi, A. & Houshmandzadeh, A., 2015. *Provenance of Neoproterozoic sedimentary basement of northern Iran, Kahar Formation.* Journal of African Earth Sciences, 111, 54-75.

Fedo, C. M., Nesbitt, H. W. & Young, G. M., 1995. *Unraveling the effects of potassium metasomatism in sedimentary rocks and paleosols, with implications for paleoweathering conditions and provenance*. Geology, *23*, 921-924.

Folk, R. L. & Ward, W. C., 1957. *Brazos River bar: a study in the significance of grain size parameters*. Journal of Sedimentary Petrology, 27, 3-26.

Folk, R. L., 1960. Petrography and *origin of the Tuscarora, Rose Hill and Keefer Formations, Lower and Middle Silurian of western West Virginia.* Journal of Sedimentary Petrology, 25, 297-301.

Garver, J. I., Royce, P. R. & Smick, T. A., 1996. *Chromium and nickel in shale of the Taconic foreland: a case study for the provenance of fine-grained sediments with an ultramafic source*. Journal of Sedimentary Research, 100, 100–106.

Garzanti, E., Vermeesch, P., Padoan, M., Resentini, A., Vezzoli, G. & Andó, S., 2014. *Provenance of passive-margin sand (Southern Africa)*. Journal of Geology, 122, 17-42.

Gazzi, P., 1966. Le arenarie del flysch sopracretaceodell' Appenninomodenese: correlazioni con il flysch di Monghidoro. Mineralogica e Petrografica, 12, 69-67.

Herron, M. M., 1988. *Geochemical classification of terrigenous sands and shales from core or log data*. Journal of Sedimentary Petrology, 58, 820-829

Kasper-Zubillaga, J. J., 2009. *Roundness in quartz grains from inland and coastal dune sands, Altar Desert, Sonora, México*. Boletín de la Sociedad Geológica Mexicana, 61, 1-12.

Kasper-Zubillaga, J. J., Armstrong-Altrin, J. S., Carranza-Edwards, A., Morton-Bermea, O., Santa-Cruz, R. I., 2013. *Control in beach and dune sands of the Gulf of Mexico and the role of nearby rivers*. International Journal of Geosciences, 4, 1157-1174.

Kasper-Zubillaga, J. J. & Carranza-Edwards, A., 2005. *Grain size discrimination between sands of desert and coastal dunes from northwestern Mexico.* Revista Mexicana de Ciencias Geológicas, 22, 383-390.

Kermani, S., Boutiba, M., Boutaleb, A. & Fagel, N., 2016. *Distribution of heavy and clay minerals in coastal sediment of Jijel, East of Algeria: indicators*

of sediment sources and transport and deposition environments. Arabian Journal of Geosciences, 9, 36. doi: 10.1007/s12517-015-2155-2.

Khan, T. & Khan, M. S., 2015. *Clastic rock geochemistry of Punagarh basin, trans-Aravalli region, NW Indian shield: implications for paleoweathering, provenance, and tectonic setting*. Arabian Journal of Geosciences, 8, 3621-3644.

Li, B., Zhuang, X., Liu, X., Wu, C., Zhou, J. & Ma, X., 2016. *Mineralogical and geochemical composition of Middle Permian Lucaogou Formation in the southern Junggar Basin, China: implications for paleoenvironment, provenance, and tectonic setting.* Arabian Journal of Geosciences, vol. 9:174. DOI 10.1007/s12517-015-2154-3.

Lozano, R. & Bernal, J. P., 2005. *Characterization of a new set of eight geochemical reference materials for XRF major and trace element analysis*. Revista Mexicana de Ciencias Geológicas, 22, 329-344.

Ma, K., Hu, S., Wang, T., Zhang, B., Qin, S., Shi, S., Wang, K. & Qingyu, H., 2017. *Sedimentary environments and mechanisms of organic matter enrichment in the Mesoproterozoic Hongshuizhuang Formation of northern China*. Palaeogeography Palaeoclimatology Palaeoecology, http://dx.doi.org/ 10.1016/j.palaeo. 2017.02.038.

Madhavaraju, J., 2015. *Geochemistry of late Cretaceous sedimentary rocks of the Cauvery Basin, south India: constraints on paleoweathering, provenance, and end Cretaceous environments*. Chemostratigraphy, 185-214. http://dx.doi.org/10.1016/B978-0-12-419968-2.00008-X.

Madhavaraju, J., Lee, Y.I., Armstrong-Altrin, J.S., & Hussain, S.M., 2006. *Microtextures on detrital quartz grains of Upper Maastrichtian-Danian rocks of the Cauvery Basin, Southeastern India: Implications for provenance and depositional environments*. Geosciences Journal, 10(1), 23-34.

McLennan, S. M., Hemming, S., McDaniel, D. K. & Hanson, G. N., 1993. *Geochemical approaches to sedimentation, provenance, and tectonics.* In: Johnson, M.J., Basu, A., (Eds.), Processes controlling the composition of clastic sediments, Geological Society of America Special Paper, 284, 21-40.

Nagarajan, R., Madhavaraju, J., Nagendra, R., Armstrong-Altrin, J. S. & Moutte, J., 2007a. *Petrography and Geochemistry of terrigenous sedimentary rocks in the Neoproterozoic Rabanpalli Formation, Bhima Basin, Southern India: Implications for Paleoweathering condition, Provenance, and Source Rock Composition.* Journal of the Geological Society of India, 70, 297-312.

Nagarajan, R., Madhavaraju, J., Nagendra, R., Armstrong-Altrin, J. S. & Moutte, J., 2007b. *Geochemistry of Neoproterozoic Shales of Rabanpalli Formation, Bhima Basin, northern Karnakata, Southern India: Implications for Provenance and paleoredox conditions.* Revista Mexicana de Ciencias Geológicas, 24, 150-160.

Nagarajan, R., Armstrong-Altrin, J. S., Kessler, F. I., Hidalgo-Moral, E. L., Dodge-Wan, D. & Taib, N. I., 2015. *Provenance and tectonic setting of Miocene siliciclastic sediments, Sibuti Formation, northwestern Borneo*. Arabian Journal of Geosciences, 8, 8549-8565.

Nesbitt, H. W. & Young, G. M., 1982. *Early Proterozoic climates and plate motions inferred from major element chemistry of lutites*. Nature, 299, 715-717.

Periasamy, V. & Venkateshwarlu, M., 2017. *Petrography and geochemistry of Jurassic sandstones from the Jhuran Formation of Jara dome, Kachchh basin, India: Implications for provenance and tectonic setting*. Journal of Earth System Science, vol. 126 (in press).

Ramos-Vázquez, M., Armstrong-Altrin, J. S., Rosales-Hoz, L., Machain-Castillo, M. L., and Carranza-Edwards, A., 2017. *Geochemistry of deep-sea sediments in two cores retrieved at the mouth of the Coatzacoalcos river delta, Western Gulf of Mexico, Mexico.* Arabian Journal of Geosciences, In press; DOI: 10.1007/s12517-017-2934-z.

Rashid, S. A. & Ganai, J. A., 2015. *Preservation of glacial and interglacial phases in Tethys Himalaya: evidence from geochemistry and petrography of Permo-Carboniferous sandstones from the Spiti region, Himachal Pradesh, India*. Arabian Journal of Geosciences, 8 (11), 9345-9363.

Rashid, S. A., Ganai, J. A., Masoodi, A. & Khan, F. A., 2015. *Major and trace element geochemistry of lake sediments, India: implications for weathering and climate control*. Arabian Journal of Geosciences, 8, 10481-10496.

Roser, B. P. & Korsch, R. J., 1986. *Determination of tectonic setting of sandstone-mudstone suites using SiO_2 content and K_2O/Na_2O ratio*. Journal of Geology, 94, 635 -650.

Roser, B. P. & Korsch, R. J., 1988. *Provenance signatures of sandstone-mudstone suites determined using discriminant function analysis of major element data*. Chemical Geology, 67, 119-139.

Selvaraj, K., Lin, B. Z., Lou, J. -Y., Xia, W. L., Huang, X. T. & Chen, C. -T. A., 2016. *Lacustrine sedimentological and geochemical records for the last 170 years of climate and environmental changes in southeastern China*. Boreas, 45, 165-179.

Tawfik, H.A., Ghandour, I.M., Maejima, W., Armstrong-Altrin, J.S. & Abdel-Hameed, A-M. T., 2017. *Petrography and geochemistry of the siliciclastic Araba Formation (Cambrian), east Sinai, Egypt: Implications for provenance, tectonic setting and source weathering.* Geological Magazine, 154(1), 1-23.

Taylor, S. R. & McLennan, S. M., 1985. *The Continental Crust: Its Composition and Evolution.* Blackwell Scientific Publications, Oxford, UK., p 1-312.

Tetiker, S., Yalçın, H. & Bozkaya, Ö., 2015. *Evidence of the diagenetic history of sediment composition in*

Precambrian-early Paleozoic rocks: a systematic study from the Southeast Anatolian Autochthon, Mardin (Derik-Kızıltepe), Turkey. Arabian Journal of Geosciences, 8, 11261-11278.

Tobia, F. H. & Aswad, K. J., 2015. *Petrography and geochemistry of Jurassic sandstones, western desert, Iraq: implications on provenance and tectonic setting*. Arabian Journal of Geosciences, 8, 2771-2784.

Van de Kamp, P. & Leake, B., 1985. *Petrography and geochemistry of feldspathic and mafic sediments of the northeastern Pacific margin*. Transactions of the Royal Society of Edinburgh, Earth Sciences, 76, 411-449.

Varga, A., Raucsik, B. & Szakmány, G., 2017. *Origin of natural arsenic antimony contents in the Permian to lower triassic siliciclastic rocks of the western Mecsek Mountains, SW Hungary*. Carpathian Journal of Earth and Environmental Sciences, 12, 5-12.

Verma, S. K., 2017. *Precambrian plate tectonic setting of Africa from multidimensional discrimination diagrams.* Journal of African Earth Sciences, 125, 137-150.

Verma, S. P. & Armstrong-Altrin, J. S., 2013. *New multi-dimensional diagrams for tectonic discrimination of siliciclastic sediments and their application to Precambrian basins*. Chemical Geology, 355, 117-180.

Verma, S. P. & Armstrong-Altrin, J. S., 2016. *Geochemical discrimination of siliciclastic sediments from active and passive margin settings*. Sedimentary Geology 332, 1-12.

Verma, S. K., Oliveira, E. P. & Verma, S. P., 2015. *Plate tectonic settings for Precambrian basic rocks from Brazil by multidimensional tectonomagmatic discrimination diagrams and their limitations.* International Geology Review, 57, 1566-1581.

Wen, H., Jiang, Y., Huang, H., Liu, Y., Wang, T., Jiang, Y., Jin, J. & Qi, L., 2016. *Provenance and diagenesis of the Upper Jurassic Qigu Formation sandstones in the southern Junggar Basin, NW China*. Arabian Journal of Geosciences, 9, 452. doi: 10.1007/s12517-016-2483-x.

Wronkiewicz, D. J. & Condie, K. C., 1990. *Geochemistry and mineralogy of sediments from the Ventersdorp and Transvaal Supergroups, South Africa: cratonic evolution during the early Proterozoic.* Geochimica et Cosmochimica Acta, 54, 343–354.

Zaid, S. M., 2015a. *Geochemistry of sands along the Ain Soukhna and Ras Gharib beaches, Gulf of Suez, Egypt: implications for provenance and tectonic setting*. Arabian Journal of Geosciences, 8, 10481-10496.

Zaid, S. M., 2015b. *Integrated petrographic, mineralogical, and geochemical study of the Late Cretaceous-Early Tertiary Dakhla shales, Quseir-Nile valley Province, central Egypt: implications for source area weathering, provenance, and tectonic setting*. Arabian Journal of Geosciences, 8, 9237-9259.

Zaid, S. M., 2015c. *Geochemistry of sandstone from the Pliocene Gabir Formation, North Marsa Alam, Red Sea, Egypt: Implication for provenance, weathering and tectonic setting*. Journal of African Earth Sciences, 102, 1-17.

Zaid, S. M., 2016. *Geochemistry of shales from the Upper Miocene Samh Formation, north Marsa Alam, Red Sea, Egypt: implications for source area weathering, provenance, and tectonic setting*. Arabian Journal of Geosciences, 9, 593. doi:10.1007/s12517-016-2623-3.

Zhang, Y. & Gao, X., 2015. *Rare earth elements in surface sediments of a marine coast under heavy anthropogenic influence: the Bohai Bay, China.* Estuarine, Coastal and Shelf Science, 164, 86-9.

Received at: 18. 03. 2017
Revised at: 26. 06. 2017
Accepted for publication at: 27. 06. 2017
Published online at: 26.07. 2017